Nonlinear Phenomena in Complex Systems, vol. **26**, no. 4 (2023), pp. 356 - 365

Analysis of Vibrational Resonance in Certain One Dimensional Nonlinear Maps Driven by an Amplitude Modulated Signal

B. Bhuvaneshwari, A. Zeenath Bazeera, S.M. Abdul Kader, and V. Chinnathambi*
Department of Physics, Sadakathullah Appa College,Tirunelveli 627 011, Tamilnadu, INDIA

S. Rajasekar
School of Physics, Bharathidasan University, Tiruchirapalli 620 024, Tamilnadu, INDIA
(Received 20 May, 2023)

The phenomenon of Vibrational Resonance (VR) is explored in the presence of an amplitude-modulated (AM) signal comprising a low-frequency component (ω) and two high-frequency components ($\Omega + \omega$) and ($\Omega - \omega$), where $\Omega >> \omega$. This investigation is conducted within the framework of certain one-dimensional nonlinear maps, specifically the Bellows map and the Bountis map. These maps are of particular interest due to their appearance in diverse physical contexts and their complex dynamical behaviors. In both the Bellows and Bountis maps, VR manifests at the low-frequency (ω) of the amplitude-modulated signal as we vary the amplitude (g) of the high-frequency signal. By carefully selecting suitable values for the high-frequency signal's amplitude (g), it becomes possible to significantly enhance the response to a weak signal. Furthermore, the maximum resonance peak is contingent upon the amplitude (g) of the amplitude-modulated signal. We characterize the VR phenomenon through the analysis of response amplitude and trajectory plots. Additionally, we explore the impact of the AM signal on various attractors within these maps, accompanied by appropriate bifurcation diagrams and Lyapunov exponent diagrams.

PACS numbers: 05.45.-a; 05.90.+m;46.40.Ff
Keywords: vibrational resonance, amplitude modulated signal, bountis map, bellows map, response amplitude
DOI: https://doi.org/10.5281/zenodo.10410049

1. Introduction

The phenomenon known as Vibrational Resonance (VR) occurs when a nonlinear system is exposed to two distinct periodic signals of significantly different frequencies, denoted as ω and Ω, where $\Omega >> \omega$. In VR, a weak low-frequency signal can be amplified by increasing the amplitude of a strong high-frequency signal. The analysis of VR has garnered considerable attention in recent years due to its wide range of applications in the fields of science and engineering. Following the pioneering work by Landa and McClintock [1], VR has been investigated in various types of systems, including neural network systems [2-4], noise-induced structures [5], optical systems [6,7], monostable systems [8], bistable systems [9-11], spatially periodic potential systems [12], excitable systems [13], time-delayed systems [14,15], groundwater-dependent ecosystems [16], coupled systems [17,18], harmonically trapped potential systems [19], and discrete dynamical systems [20,21].

Motivated by prior research findings, this paper presents a numerical investigation into the occurrence of Vibrational Resonance (VR) within specific one-dimensional nonlinear maps, namely the Bellows map and the Bountis map, when subjected to an amplitude-modulated (AM) signal. Discrete-time systems, described

*E-mail: veerchinnathambi@gmail.com

by nonlinear difference equations, are often preferred for their practicality and reliability over continuous-time differential equations. They yield efficient computational results for numerical simulations and offer a richer dynamic range compared to continuous systems. The use of amplitude-modulated signals finds wide application across engineering and scientific domains [22-27], making it an essential topic for enhancing weak signals in modulated form. Given our objective to analyze the VR phenomenon in two one-dimensional maps under the influence of an amplitude-modulated signal, we express the AM signal as follows:The equation for the amplitude-modulated (AM) signal is given by:

$$S(n) = [f + 2\ g\ \cos\omega n]\sin\omega n, \tag{1.1}$$

which can also be written as

$$S(n) = f\sin\omega n + g\sin(\Omega+\omega)n + g\sin(\Omega-\omega)n, \tag{1.2}$$

where f and g denote the amplitudes of the AM signal, and ω and Ω represent the two frequencies of the AM signal with $\omega << \Omega$. In Equation (1), $f\sin\omega n$ represents the carrier signal, which is modulated by the other harmonic signal $g\cos\Omega n$. Furthermore, it is important to note that the signal satisfies $f << 1$ and $\omega << \Omega$.

The remainder of this paper is structured as follows: Firstly, in Section 2, we provide introductions to both maps, namely the Bellows map and the Bountis map. In Section 3, we conduct a numerical analysis to investigate the occurrence of Vibrational Resonance (VR) within the Bellows map when driven by the AM signal. Next, in Section 4, we extend our analysis to explore the occurrence of VR within the Bountis map under the influence of the AM signal. Finally, our concluding remarks are presented in Section 5.

2. One Dimensional Maps

The general form of a one-dimensional map is expressed as:

$$X_{n+1} = f(X_n) \tag{2.1}$$

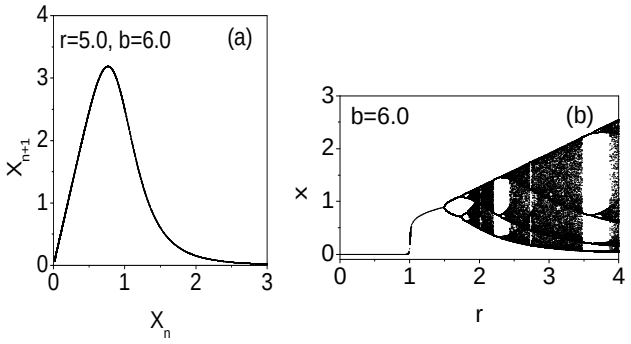

FIG. 1. (a) Return map of the Bellows map for $r = 5.0$ and $b = 6.0$ (b) Bifurcation diagram of the Bellows map for $r = 2.0$ and $b = 6.0$.

Here, X_{n+1} is a function of the discrete variable X at the previous (n^{th}) iteration, influenced by certain parameters. Historically [28,29], X_n has been employed to represent the population density of an organism at the n^{th} generation. When the function $f(X_n)$ exhibits the tendency to increase monotonically as X is small and decrease monotonically as X becomes large, often due to density-dependent processes, it assumes a characteristic "hump"-like shape characterized by a unique maximum. In our current research, we select two specific one-dimensional maps featuring such hump functions.

(i) Bellows Map

First, we examine the Bellows map [30-32], described by the following difference equation:

$$X_{n+1} = f(X_n) = \frac{rX_n}{1 + X_n^b} \tag{2.2}$$

This map serves as a model for the evolution of population density within an organism, where the parameter r is associated with environmental factors. The equilibrium points of this map are at 0 and $(r-1)^b$. The critical point, denoted as the point where $f'(X) = 0$, occurs at $(\frac{1}{b-1})^{1/b}$. Specifically, for $b = 2$, Equation (4) possesses only one fixed point, $X^* = 0$, for values of r between 0 and 1. However, for $r > 1$, it exhibits three fixed points, with $X_0^* = 0$ being unstable and $X_\pm^* = \pm\sqrt{r-1}$ being stable. In other words, the Bellows map assumes a monostable state when $0 < r \leq 1$ and transitions to a

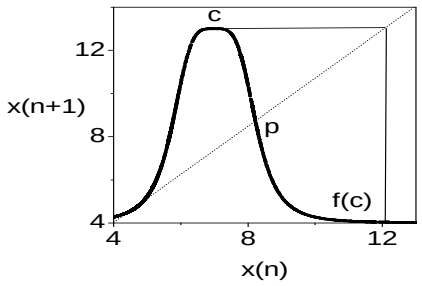

FIG. 2. x_n versus x_{n+1} plot of Bountis map for $\xi = 20.0$ and $\mu = 5.0$. The other parameters values are fixed as $l = m = 4.0, a = 3.0, r = 0.6, s_1 = 1.5, s_2 = 0.12$ and $c = 7.0$ respectively.

bistable state when $r > 1$. Figures 1(a) and 1(b) depict the return map (X_n versus X_{n+1}) and the bifurcation diagram as r increases for the Bellows map. Figure 1(a) vividly illustrates the characteristic "inverted U-shape" or hump-like nature of the nonlinear function $f(X)$ in the return map. In Fig. 1(b), the Bellows map exhibits various dynamic behaviors, including transcritical bifurcation, period-doubling leading to chaotic behavior, periodic windows, and intermittent behavior.

(i) Bountis Map The difference equation defining the Bountis map is as follows [33]:

$$x_{n+1} = a + \frac{(\xi - \mu) + r(x - c)^l}{s_1 + s_2\mu(x - c)^m}, \quad m \geq l, \quad a > 0. \tag{2.3}$$

Here, $\mu, \xi, l, m, a, r, s_1, s_2$, and c represent various parameters. Raghavan *et al.* [33] conducted a numerical study to explore the existence of reversal in period-doubling sequences and antimonotonic behavior within the Bountis map.

First, let's analyze the important features of this map. Figure 2 displays the return map (x_n versus x_{n+1} plot) of the Bountis map with $\xi = 20.0$ and $\mu = 5.0$. This figure vividly illustrates the distinctive "inverted U shape" (hump) nature of the $f(x)$ nonlinear function in the return map. From the return map of the Bountis map, we can observe the following key features: (i) A non-zero origin. (ii) A unique smooth maximum point with inflection points on either side of it. (iii) An asymptotic long tail to the right of the maximum. (iv) For small values of ξ and an appropriate choice of a, there are no fixed points in the interval $[0, c]$. (v) When $\xi = 20$, the map has only one fixed point, denoted as P, which falls within the interval $[c, f(c)]$. However, for large values of ξ, multiple fixed points appear within the interval $[0, c]$.

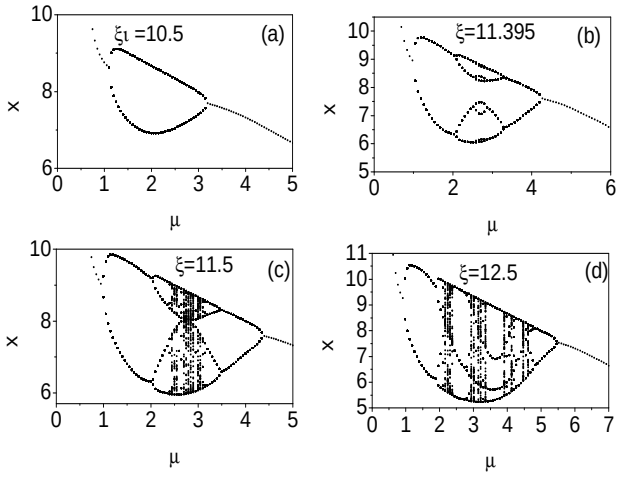

FIG. 3. Bifurcation diagrams of Bountis map for certain values of ξ (a) Bubble structure at $\xi = 10.5$ (b) Cascading of period-doubling with bubble structure at $\xi = 11.395$ (c) Chaotic states with bubble structure at $\xi = 11.5$ (d) Period adding sequences with reversal of period doubling sequences at $\xi = 12.5$. The other parameters values are fixed as $l = m = 4.0, a = 3.0, r = 0.6, s_1 = 1.5, s_2 = 0.12$ and $c = 7.0$ respectively.

Next, we conduct a numerical analysis to investigate the presence of various dynamic behaviors, such as antimonotonicity and chaos, in the Bountis map. For our numerical study, we maintain the parameter values at $l = m = 4.0$, $a = 3.0$, $r = 0.6$, $s_1 = 1.5$, $s_2 = 0.12$, $c = 7.0$, while allowing μ and ξ to be control parameters. The bifurcation diagram of the Bountis map, where we vary the control parameter μ while keeping a few values of ξ constant, is presented in Fig. 3. Specifically, Fig. 3(a) illustrates the bifurcation diagram of μ versus x for $\xi = 10.5$. As μ increases, the system described by Eq. (2)

remains in a periodic state, following the pattern: Period-1 $\rightarrow$ Period-2 $\rightarrow$ Period-1, thus forming a primary bubble structure. With a further increase in ξ, the number of nested bubbles grows exponentially as 2^n with $n = 1, 2, 3, ...$ This exponential growth is clearly evident in Fig. 3(b) for $\xi = 11.395$. As μ continues to increase, chaotic states begin to emerge. This is clearly observed in Figs. 3(c) and 3(d), which depict the bifurcation diagram of μ versus x for $\xi = 11.5$ and $\xi = 12.5$ respectively. The once-structured bubble pattern now exhibits chaotic behavior, and as μ increases further, these chaotic states become more pronounced. As we raise the values of ξ we can observe period-adding sequences with fold bifurcations at the accumulation point of periodic windows.

3. Resonance in the Bellows map with AM signal

The Bellows map, driven by an AM (Amplitude Modulated) signal, is described by the following equation:

$$X_{n+1} = f(X_n) = \frac{rX_n}{1 + X_n^b} + S(n) \tag{3.1}$$

Here, $S(n)$ represents the AM signal. We conduct an analysis of this map (Eq. 6) under specific parameter settings that place the system within a bistable regime. We keep the parameters fixed at $b = 2.0$, $r = 2.0$, $f = 0.1$, $\omega = 0.1$, and $\Omega = 1.0$. The amplitude g of the high-frequency signal serves as the control parameter. Since this is a discrete-time system, the maximum frequency we can apply is limited to $\Omega = \pi$. Initially, when $g = 0$, the system exhibits two coexisting attractors, one centered around the fixed point X_+^* and another around X_-^*. Moreover, at this value of g, there is no interplay or motion between these two attractors. We perform iterations of the map, starting with an initial value X_0, discarding the first 10^4 iterations as transient. The solution of the map inherently comprises both a slow motion with frequency ω and a fast motion with frequency Ω.

We concentrate our analysis on the low-frequency component of the output signal, which exhibits resonance. From the numerical solution of x_n, the response amplitude Q is computed through $Q = \sqrt{Q_s^2 + Q_c^2}/f$, at the signal frequency (ω), where

$$Q_s = \frac{2}{NT} \sum_{n=1}^{NT} x_n \sin\omega n, \tag{3.2}$$

$$Q_c = \frac{2}{NT} \sum_{n=1}^{NT} x_n \cos\omega n, \tag{3.3}$$

where $T = 2\pi/\omega$ and N is very large. In our numerical calculation of Q, N is chosen as 10^3.

In Figure 4(a), we depict the variation of numerically calculated Q with respect to g for four values of r: $r = 0.75, 1.0, 1.5$, and $r = 2.0$. The other parameters are held constant at $\omega = 0.1$, $\Omega = 1.0$, $b = 2.0$, and $f = 0.1$. Notably, for $r \leq 1$, no resonance is observed, and in such cases, the response amplitude Q exhibits a monotonically decreasing behavior with respect to g. It's worth noting that for $r \leq 1$, the map possesses only one fixed point at $x^* = 0$. For $r = 1.5$, two resonances emerge. The first resonance occurs at $g = 0.22757$ with $Q_{max} = 8.260$, and the second resonance manifests at $g = 0.96024$ with $Q_{max} = 2.2323$, as clearly shown in Figure 4(a). Similarly, for $r = 2.0$, we observe two resonances. The first resonance materializes at $g = 0.38029$ with $Q_{max} = 11.7123$, while the second resonance occurs at $g = 1.2553$ with $Q_{max} = 3.6249$. When the map is subjected to a biharmonic signal, a single resonance peak is observed for all values of r. Interestingly, in contrast to this result, when the map is subjected to an AM signal, two resonance peaks emerge for $r > 1$. Furthermore, as the control parameter r increases, both Q_{max} and the positions of the resonance peaks shift towards higher values of g, as indicated by the increasing values of r. In Figure 4(b), we analyze the resonance pattern for different values of Ω (the frequency of the high-frequency signal), specifically $\Omega = 1.0, 1.5$, and 2.0, while keeping $r = 2.0$ constant. For all values of Ω,

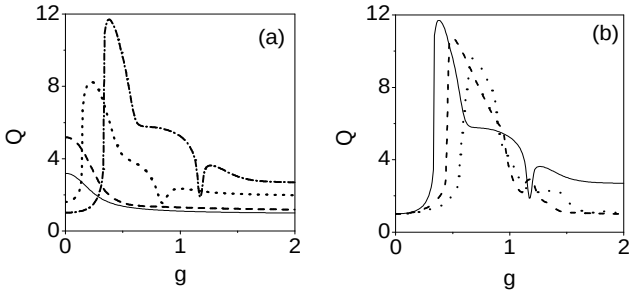

FIG. 4. The variation of the response amplitude Q as a function of the control parameter g (a) with $\omega = 0.1, \Omega = 1.0, f = 0.1$ and four values of r. The values of the solid, dashed, dotted and dashed dot curves are 0.5,1.0,1.5 and 2.0 (b) with $f = 0.1, r = 2.0, \omega = 0.1$ and three values of Ω such as $\Omega = 1.0$ (solid curve), $\Omega = 1.5$ (dashed curve) and $\Omega = 2.0$(dotted curve.

we observe double resonances. However, the maximum of the response amplitude Q_{max} decreases as Ω increases, and the positions of the resonance peaks shift towards higher values of g with increasing Ω. For instance, in Figure 4(b), for $\Omega = 1.0, 1.5, 2.0$, the first resonances occur at $g = 0.38029, 0.49525, 0.6691$, with corresponding Q_{max} values of $11.7123, 10.6999, 9.5983$. The second resonances occur at $g = 1.2553, 1.1775, 1.4063$, with Q_{max} values of $3.6249, 2.8508, 2.2888$.

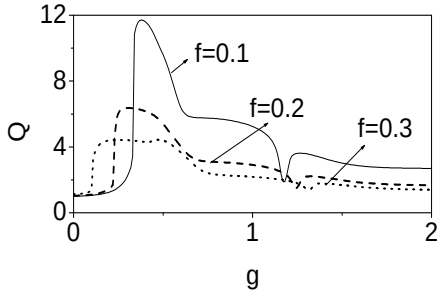

FIG. 5. The variation of the response amplitude Q as a function of the control parameter g with $r = 2.0, \omega = 0.1, \Omega = 1.0$ and three values of f. The values of the solid, dashed and dotted curves are 0.1,0.2 and 0.3.

In Figure 5, we present the variation of Q with respect to g for three values of f: $f = 0.1, 0.2, 0.3$, while keeping $r = 2.0$ constant. Double resonances occur for $f = 0.1$ (solid curve) and 0.2 (dashed curve), and three resonances are observed for $f = 0.3$ (dotted curve), as clearly depicted in Figure 5. Notably, Q_{max} decreases with an increase in the value of f. Specifically: For $f = 0.1$, resonances occur at $g = 0.38029$ with $Q_{max} = 11.7123$ and at $g = 1.2553$ with $Q_{max} = 3.6249$. For $f = 0.2$, resonances manifest at $g = 0.26939$ with $Q_{max} = 6.1777$ and at $g = 1.31029$ with $Q_{max} = 2.1325$. For $f = 0.3$, three resonances occur at $g = 0.16502$ with $Q_{max} = 4.19746$, $g = 0.51363$ with $Q_{max} = 4.0542$, and $g = 1.3554$ with $Q_{max} = 1.76023$. Additionally, the positions of the resonance peaks shift towards lower values of g with increasing f.

Moving on, we present the bifurcation diagram of the Bellows map (Eq. 6) in Figure 6(a) and the corresponding maximal Lyapunov exponent diagram in Figure 6(b) for $r = 2.0$. The values of the other parameters are set to $b = 2.0$, $f = 0.1$, $\omega = 0.1$, and $\Omega = 1.0$. The Lyapunov exponent λ is defined as:

$$\lambda = \lim_{N\to\infty} \frac{1}{NT} \sum_{n=1}^{NT} ln \mid f'(X_n) \mid . \qquad (3.4)$$

Figure 6 shows that the Lyapunov exponent λ remains negative across the entire range of g values, implying that the time series of the map is periodic. However, it is noteworthy that the Bellows map exhibits a variety of bifurcations without the AM signal, as evident in Figure 1(b). This observation suggests that chaos is suppressed due to the presence of the AM signal in the Bellows map. In Figure 4(a), with parameters set to $r = 2$, $f = 0.1$, $\Omega = 1.0$, and $\omega = 0.1$, the first resonance occurs at $g = 0.38029$, and the second resonance occurs at $g = 1.2553$. To better understand the mechanism behind these resonances, we examine the time series plots. Figure 7 illustrates the behavior of x_n for four different values of g while keeping $r = 2$ constant. For $g = 0.0$ (Figure 7(a)), two coexisting oscillating solutions are evident, with one near x_+ and the other near x_-. As g deviates from zero, even for small values, two oscillating solutions persist. However, these solutions are modulated

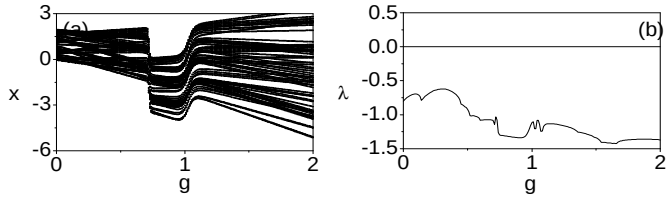

FIG. 6. (a) Bifurcation diagram (x_n versus g) of Bellows map driven by an AM signal and (b) the variation of Lyapunov exponent λ for $r = 2.0$. The values of the other parameters are $b = 2.0, \omega = 0.1, \Omega = 1.0$ and $f = 0.1$.

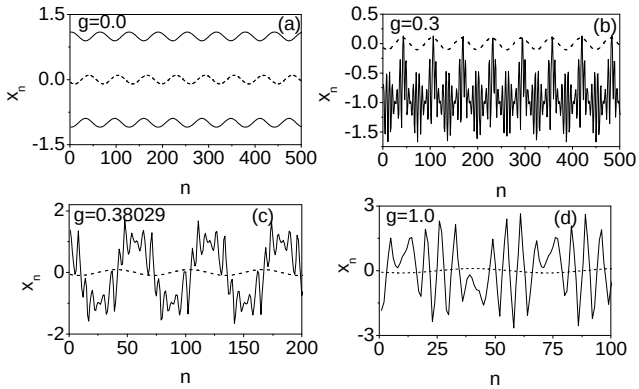

FIG. 7. x_n versus n (continuous curve) for a few values of g with $r = 2.0$. The dashed curve represents the periodic signal $f \sin \omega n$. Resonance curve occurs at $g = 0.38029$. The simulation parameters are $b = 2.0, f = 0.1, \Omega = 1.0$ and $\omega = 0.1$.

by the high-frequency signal $f \cos(\Omega n)$. This type of behavior is observed for $g < 0.3$. At $g = 0.3$ (Figure 7(b)), x_n switches between regions $x < 0$ and $x > 0$ around the two fixed points, but the residence times of the trajectories in these regions differ. Periodic switching between the two fixed points occurs precisely at $g = 0.38029$, as clearly shown in Figure 7(c). At this value of g, the response amplitude Q reaches its maximum. The crossing of x_n from $x < 0$ to $x > 0$ occurs when the input signal $f \sin(\omega n)$ reaches its maximum. At $g = 1.0$ (which is far from resonance), the mean residence times in the regions $x < 0$ and $x > 0$ decrease, leading to rapid switching between these regions around the two fixed points, as depicted in Figure 7(d).

4. Vibrational Resonance in the Bountis Map

In the previous section, we explored the occurrence of Vibrational Resonance (VR) in the Bellows map when driven by an AM signal. In this section, we turn our attention to the investigation of VR in the Bountis map when subjected to an AM signal. The difference equation describing the Bountis map with an AM signal is as follows:

$$x_{n+1} = f(x_n; \mu, \xi) = a + \frac{(\xi - \mu) + r(x - c)^l}{s_1 + s_2 \mu (x - c)^m} + S(n) \,, \tag{4.1}$$

We analyze the response amplitude Q by employing Eqs. (7) and (8) while varying the amplitude g for several values of a, Ω, and f. The following parameters are held constant: $l = m = 4.0, r = 0.6, s_1 = 1.5, s_2 = 0.12, c = 7.0, \mu = 4.0$, and $\xi = 7.99$. The evolution of the response amplitude Q concerning the high-frequency signal amplitude g is presented in Figure 8 for four values of a: $a = 1.0, 2.0, 3.0$, and 4.0, while maintaining $\omega = 0.1, \Omega = 1.0$, and $f = 0.1$. In Figure 8(a), for $a = 1.0$ (solid line), no resonance is observed, and in this case, Q increases monotonically with increasing g. A single resonance is evident for $a = 2.0$ (dashed line) at $g = 1.3732$ with $Q_{max} = 1.4646$. Double resonances occur for $a = 3.0$ (dotted line) and $a = 4.0$ (dashed dot line), as clearly shown in Figure 8(a). Specifically, for $a = 3.0$, the first and second resonances occur at $g = 0.7297$ with $Q_{max} = 1.7524$ and $g = 1.2534$ with $Q_{max} = 1.3438$. For $a = 4.0$, the first and second resonances materialize at $g = 0.42089$ with $Q_{max} = 1.988$ and $g = 1.19589$ with $Q_{max} = 1.385$. Notably, the maximum of the resonance curve increases as the control parameter a increases, while its location shifts toward lower values of the higher frequency amplitude g.

Figure 8(b) presents the variation of numerically computed Q against the control parameter g for several values of Ω: $\Omega = 1.0, 2.0$, and 3.0, while keeping $a = 3.0, f = 0.1$, and $\omega = 0.1$. In Figure 8(b), for $\Omega = 1.0$ (solid line),

resonances occur at two places: $g = 0.7297$ with $Q_{max} = 1.7524$ and $g = 1.2534$ with $Q_{max} = 1.3438$. However, for $\Omega = 2.0$ and $\Omega = 3.0$, only one resonance is observed at $g = 1.0455$ with $Q_{max} = 1.5694$ and $g = 0.9585$ with $Q_{max} = 1.4061$. From Figure 8(b), it is observed that the maximum of the response amplitude decreases with an increase in Ω, and its location shifts toward higher values of g. The bifurcation pattern for the Bountis map with an AM signal described by Eq. (10) is depicted in Figure 9(a). The corresponding Lyapunov exponent diagram is shown in Figure 9(b). It is clearly evident that with the inclusion of the AM signal, attractors disappear, and the system exhibits periodic and chaotic behaviors, instead of following a reverse period doubling route to chaos.

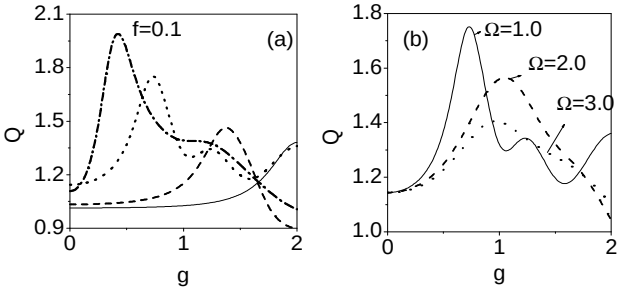

FIG. 8. The variation of the response amplitude Q as a function of the control parameter g (a) with $\omega = 0.1, \Omega = 1.0, f = 0.1$ and four values of a. The values of the solid, dashed, dotted and dashed dot curves are 1.0,2.0,3.0 and 4.0 (b) with $f = 0.1, a = 3.0, \omega = 0.1$ and three values of Ω such as $\Omega = 1.0$ (solid curve), $\Omega = 2.0$ (dashed curve) and $\Omega = 3.0$(dotted curve).

Figure 10 illustrates the variation of numerically computed Q with respect to the amplitude g of the high-frequency signal for three values of f: $f = 0.1, 0.2, 0.3$, while keeping $a = 3.0$. For all values of f, as g increases from 0, the value of Q also increases until reaching a maximum value, after which it decreases with further increases in g. Interestingly, the maximum value of the peak is detected at two positions for $f = 0.1$, whereas only a single peak is observed for $f > 0.1$, as clearly shown in Figure 10. It's worth noting that for all values of f, the first resonance

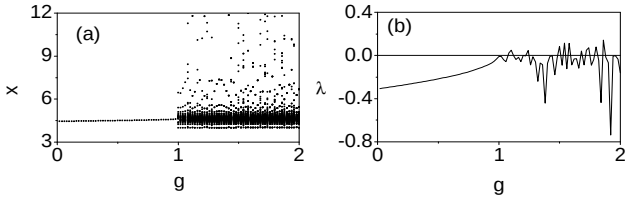

FIG. 9. (a) Bifurcation diagram (x_n versus g) of Bountis map driven by an AM signal and (b) the variation of Lyapunov exponent λ for $a = 3.0$. The values of the other parameters are $b = 2.0, \omega = 0.1, \Omega = 3.0$ and $f = 0.1$.

occurs at nearly the same value of g, specifically at $g = 1.7524$. However, the maximum of the resonance curve, denoted as Q_{max}, decreases as f increases, as evident in Figure 10. In addition, we analyzed the motion of x_n corresponding to the resonance shown in Figure 10 for $f = 0.1$ (solid line). We accomplished this by plotting time series plots for four values of g. The simulation parameters used for this analysis are $a = 3.0, \omega = 0.1, \Omega = 1.0$, and $f = 0.1$. When $g = 0.0$, the map is driven by a pure sinusoidal signal, resulting in a sinusoidal pattern observed in Figure 11(a). However, as g increases, the modulation of x_n by the high-frequency signal grows, leading to an amplitude-modulated pattern, as clearly seen in Figures 11(b) to 11(d).

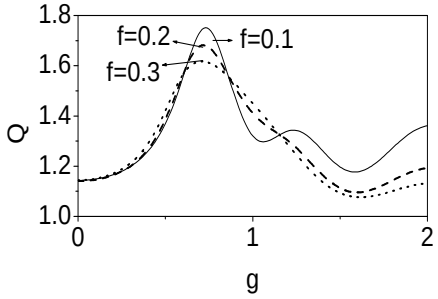

FIG. 10. The variation of the response amplitude Q as a function of the control parameter g with $\omega = 0.1, \Omega = 1.0, f = 0.1$ and three values of f. The values of the solid, dashed and dotted curves are $f = 0.1, 0.2$ and 0.3.

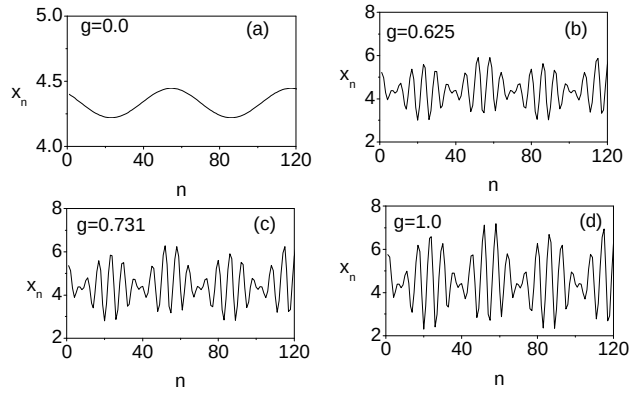

FIG. 11. x_n versus n plot for a few values of g. The simulation parameters are $a = 3.0, f = 0.1, \Omega = 1.0$ and $\omega = 0.1$.

5. Conclusion

In this study, we conducted numerical investigations into the occurrence of vibrational resonance (VR) in two nonlinear maps: the Bellows map and the Bountis map, when subjected to the influence of an amplitude-modulated signal with $\omega << \Omega$. In both maps, resonance at the low-frequency ω is induced by the high-frequency component of the amplitude-modulated signal, leading to a significant enhancement of the weak signal. Our numerical analysis revealed the presence of VR in both maps within certain ranges of parameter values. In the Bellows map, resonance results in periodic switching between two coexisting states. Beyond the resonance, the mean residence times in regions $x < 0$ and $x > 0$ decrease, leading to rapid switching between these regions. In the Bountis map, for small values of g, x_n oscillates around the fixed point regardless of g. As g increases, the modulation of x_n by the high-frequency signal evolves into a modulated wave pattern. In the absence of an amplitude-modulated signal, both maps exhibit a variety of bifurcations, including periodic doubling, reverse period-doubling, antimonotonicity, period-adding sequences, flip bifurcation, and more. However, the presence of the AM signal causes the Bellows map to display quasiperiodic behavior and the Bountis map to exhibit periodic and chaotic behaviors within specific ranges of parameter values. Exploring other types of resonances in these maps with amplitude-modulated signals, as described by Eqs. (6) and (10), may yield further intriguing results.

References

[1] P.S. Landa and P.V.E. McClintock. Vibrational Resonance. J.Phys. Math. Gen., **33**, L433-L438 (2000). DOI https://doi.org/10.1088/0305-4470/33/45/103

[2] B. Deng, J. Wang, X.L. Wei, K.M. Tsang and W.L. Chan. Vibrational Resonance in neuron populations. Chaos: An interdisciplinary Journal of Nonlinear science, **20(1)**, 013113 (2010). https://doi.org/10.1063/1.3324700

[3] Y.M. Qin, J. Wang, C. Men, B. Deng and X.L. Wei. Vibrational Resonance in feedforward network. Chaos: An interdisciplinary Journal of Nonlinear science, **21(2)**, 023113 (2011). https://doi.org/10.1063/1.3603818

[4] J.B. Sun, B. Deng, C. Liu, H.T. Yu, J. Wang and X.L. Wei. Vibrational resonance with in neuron populations with Hybrid Synapses. Applied Mathematical Modelling, **37(9)**, 6311-6324 (2015). https://doi.org/10.1016/j.apm.2013.01.007

[5] A.A. Zaikin, L. Lopez, J.P. Baltanas, J. Kurths and M.A.F. Sanjuan. Vibrational Resonance in a Noise-induced Structure. Phys. Rev. E, **66(1)**, 011106 (2002). DOI:https://doi.org/10.1103/PhysRevE.66.011106

[6] V. N. Chizhevsky, E. Smeu and G. Giacomelli. Experimental Evidence of Vibrational Resonance in an Optical system. Phys. Rev. Letters, **91(22)**, 220602 (2003). DOI:https://doi.org/10.1103/PhysRevLett.91.220602

[7] V.N. Chizhevsky and G. Giacomelli. Experimental and Theoretical Study of the noise-induced gain degradation in Vibrational resoanace. Phys. Rev. E, **70**, 062101 (2004). DOI:https://doi.org/10.1103/PhysRevE.70.062101

[8] S. Jeyakumari, V. Chinnathambi, S. Rajasekar and M.A.F. Sanjuan. Single and Multiple Vibrational Resonance in a Quintic Oscillator in the Monostable Potentials. Physical Review E, **80**, 046608 (2009). DOI:https://doi.org/10.1103/PhysRevE.80.046608

[9] M. Gitterman. A Bistable Oscillator Driven by Two Periodic Fields. J.Phys.A, **34**, L355-L357 (2001). DOI https://doi.org/10.1088/0305-4470/34/24/101

[10] J.P. Baltanas, L. Lopez, I. Blechman, P.S. Landa, A. Zaikin and J. Kurths. Experimental Evidence, Numerics, and Theory of Vibrational Resonance in Bistable Systems. Phys. Rev. E, **67**, 066119 (2003). DOI:https://doi.org/10.1103/PhysRevE.67.066119

[11] I.I. Blckhman and P.S. Landa. Conjugate Resonances and Bifurcations in Nonlinear Systems Under Biharmonical Excitation. Int. J. Non-Linear Mech., **39**, 421-426 (2004). DOI 10.1016/S0020-7462(02)00201-9

[12] S. Rajasekar, K. Abirami and M.A.F. Sanjuan. Novel Vibrational Resonance in Multistable Systems. Chaos, **21**, 033106 (2011). https://doi.org/10.1063/1.3610213

[13] E. Ullner, A. Zaikin, J. Garcia-Ojalvo, R. Bascons and J. Kurths. Vibrational resonance and Vibrational propagation in excitable system. Phys.Lett. A, **312**, 348-354 (2003). https://doi.org/10.1063/1.3076396

[14] J.H. Yang and X.B. Liu. Delay Induces Quasi-periodic Vibrational Reosnance. J. Phys. A: Math. Theor., **43**, 122001 (2010). DOI https://doi.org/10.1088/1751-8113/43/12/122001

[15] C. Jeevarathinam, S. Rajasekar and M.A.F. Sanjuan. Theory and Numerics of Vibrational Resonance in Duffing Oscillator with Time Delayed Feedback. Physical Review E, **8**, 066205 (2011). DOI:https://doi.org/10.1103/PhysRevE.83.066205

[16] C. Jeevarathinam, S. Rajasekar and M.A.F. Sanjuan. Vibrational Resonance in Groundwater-Dependent Plant Ecosystems. Ecological Complexity, **15**, 1-37 (2013). http://dx.doi.org/10.1016/j.ecocom.2013.02.003

[17] C. Yao and M. Zhan. Signal Transmission by Vibrational Resonance in One-way Coupled Bistable Systems. Phys. Rev. E, **81**, 061129 (2010). DOI:https://doi.org/10.1103/PhysRevE.81.061129

[18] V.M. Gandhimathi, S. Rajasekar and J. Kurths. Vibrational and Stochastic Resonances in Overdamped two Coupled Anharmonic Oscillators. Phys. Lett. A, **360**, 279-286 (2006). DOI: 10.1088/0031-8949/76/6/019

[19] K. Abirami, S. Rajasekar and M.A.F. Sanjuan. Vibrational resonance in a harmonically trapped potential system. Commun Nonlinear Sci Numer Simult., **47**, 370-378 (2017). http://dx.doi.org/10.1016/j.cnsns.2016.12.002

[20] S. Rajasekar, J. Used, A. Wagemakers and M.A.F. Sanjun. Vibrational Resonance in Biological Nonlinaer Maps. Communications in Nonlinear Science and Numerical Simulation, **17**, 3435-3445 (2012). DOI: 10.1016/j.cnsns.2011.12.014

[21] A. Jeevarekha, M. Santhiah, P. Philominathan. Enriched Vibrational in Certain Discrete System. Pramana J of Phys., **83(4)**, 493-504 (2014).DOI: 10.1007/s12043-014-0815-5

[22] J. Juutilainen and R. de Seze. Biological effects of amplitude modulated radiofrequency radiation. Scan. J. Work Env. & Health, **24(4)**, 245-254 (1998). DOI: 10.5271/sjweh.317

[23] M. Siewe Siewe, C. Tchawoua and S. Rajasekar. Homoclinic bifurcation and chaos in ϕ^6-Rayleigh oscillator with three wells driven by an amplitude modulated force. Int. J. Bifur. & Chaos, **21(6)**, 1583-1593 (2011). https://doi.org/10.1142/S0218127411029288

[24] L.E. Medina and W.M. Grill. Nerve excitation using an amplitude modulated signal with kilohertz-frequency carrier and non-zero offset. J. Neuro Eng. Rehab., **13**, 63 (2016). https://doi.org/10.1186/s12984-016-0171-4

[25] Y.A. Amer, S.M. Ahmed, M.M. Dahshan and N.M. Ali. Dynamical chaos in ϕ^6-Rayleight oscillator with three wells driven an amplitude modulated force. J. Adv. Maths., **12(8)**, 6545-6551 (2016).

[26] Y. Shi. Melnikov analysis of chaos and heteroclinic bifurcation in Josephson system driven by an amplitude-modulated force. Int. J. Dynam. Control, **6(2)**, 589-600 (2018). DOI: 10.1007/s40435-017-0340-8.

[27] Y. Yu, Q. Wang, Q. Bi and C.W. Lim. Multiple-S-shaped critical manifold and jump phenomena in low frequency forced

vibration with amplitude modulation. nt. J. Bifur. & Chaos, **29(5)**, 1930012 (2019). https://doi.org/10.1142/S021812741930012X.

[28] R.M May. Simple mathematical models with very complicated dynamics. Nature, **261**, 459-467 (1976). https://doi.org/10.1038/261459a0

[29] M J Feigenbaum. Quantitative Universality for a Class of Nonlinear Transformations. J. Star. Phys., **19**, 25 (1978).

[30] T.S. Bellows. The descriptive properties of some models for density dependence. J. Anim. Ecol., **50**, 139-156 (1981). https://www.jstor.org/stable/4037.

[31] K. Masutani. Effects of survival thresholds upon one-dimensional dynamics of single-species populations. Bull, Math. Biol., **55**, 1-14 (1993). https://doi.org/10.1016/S0092-8240(05)80059-X.

[32] S. Sinha and P.K Das. Dynamics of simple one-dimensional maps under perturbation. Pramana J. Phys., **48**, 87-98 (1997). https://doi.org/10.1007/BF02845624

[33] R. Raghavan and G. Ananthakrishna. Long Tailed Map as a Representaion of Mixed Mode Oscillatory Systems. Physica D, **211**, 74-87 (2005). http://dx.doi.org/10.1016/j.physd.2005.08.004.